Eur. Phys. J. Plus (2020) 135:685
https://doi.org/10.1140/epjp/s13360-020-00643-x

THE EUROPEAN PHYSICAL JOURNAL PLUS

Regular Article

Rough curved microchannel slip flow

Nnamdi Fidelis Okechi[1,a], **Saleem Asghar**[2]

[1] Mathematics Programme, National Mathematical Centre, Abuja, Nigeria
[2] Department of Mathematics, COMSATS University Islamabad, Islamabad, Pakistan

Received: 20 January 2020 / Accepted: 28 July 2020 / Published online: 30 August 2020
© Società Italiana di Fisica and Springer-Verlag GmbH Germany, part of Springer Nature 2020

Abstract This paper models a slip flow through a curved microchannel. The curved walls confining the flow have surface roughness of small amplitude. Through domain perturbation analysis, the analytical expression of the volumetric flow rate is obtained as a function of the Knudsen number of the slip flow, the channel radius of curvature and the parameters characterising the surface roughness. It is found that the surface roughness effect is decreased in the slip regime compared to the continuum case. The study further shows that the volumetric flow rate can be enhanced, depending on roughness parameters. The channel radius of curvature has a significant effect on the entire flow.

1 Introduction

Flow dynamics in microchannels have been studied by researchers, diversely and intensively, due to the developments in the area of microfabrication technology. The advancement in this research field is well accompanied by many significant applications, including microsensors and microdevices [1–5], biofluid mechanics [6, 7], and vacuum technology [8]. The understanding of the flow behaviour in microchannels is central to the design of microelectromechanical systems (MEMS).

Studies have shown that the behaviours of flow in microdomains are considerably distinct from those observed in macrodomains [9–14]. For microchannel flows, the mean free path is comparable to the characteristic dimension of the channel. Thus, the microscopic effect is significant, compared to macrochannel flows. In a microchannel, the fluid–wall interactions exhibit non-continuum phenomena, due to rarefaction effect. Consequently, a slip regime exists, where velocity slip for isothermal flows [14, 15] and temperature jump for non-isothermal flows [16] are encountered at the flow walls. In the slip regime, the non-continuum phenomenon at the walls can be described by slip wall conditions expressed using the Knudsen number (Kn), where the Knudsen number denotes the ratio of mean free path to characteristic length scale of the microchannel. For low Knudsen number ($0.001 < \mathrm{Kn} \leq 0.1$), the flow in the microchannel is reasonably governed by continuum conservation equations, whereas the wall conditions are modelled by a non-continuum approach to describe the fluid–wall interactions [17].

The limitations in macrofabrication technology lead to the presence of distributed roughness on the walls of microchannels, fabricated via several micromachining techniques. The

[a] e-mail: okechinnamdi@hotmail.com (corresponding author)

wall roughness alters the flow geometry, such that the flow characteristics are modified depending on the parameters characterising the roughness. To demystify the physics associated with the rough microchannel flows, several researches have been carried out in the literature. Chu [18] evaluated a viscous flow through a rough straight microchannel with slip impact, and it was shown that in the slip regime, the flow rate is determined by the Knudsen number and the roughness parameters. Li et al. [19] considered the effect of roughness on rarefied gas flow in long microtubes, in the presence of a porous material. Sun and Faghri [20] discussed the effect of relative roughness, the distribution of roughness and the Knudsen number on nitrogen flow in microchannel. The friction coefficient of rarefied gas flow in the rough microchannel flow was found to be higher compared to gas flow in a smooth channel, without roughness. Duan and Muzychka [21] studied the laminar flows in a rough microtube, under no-slip and slip phenomena. The effect of roughness was found to be prominent under both phenomena; the pressure drop was shown to be increased by the roughness. The authors also showed that the velocity slip decreases the pressure drop. Garg and Agrawal [22] numerically studied the friction factor for a gaseous slip flow in a microchannel with micro-ridges, where the micro-ridges form a structured roughness on the wall surface of the microchannel. The authors further performed experiments to investigate subsonic choking in slip regime by structured roughness in microchannels [23, 24]. The aforementioned studies examined slip flows through rough straight microchannels, where the effect of channel curvature on the flows is not considered. In applications, curved microchannels are encountered, for example, in MEMS, thus studying curved microchannel flows is imperative and fundamental to understanding the inherent flow characteristics.

Furthermore, steady and unsteady flows in rough curved channels have been studied by Okechi and Asghar [25–27] and Okechi et al. [28] with continuum assumption at rough walls confining the flow. However, in the slip regime, the flow behaviour in rough curved microchannel cannot be predicted by the conventional flow models [25–28], which are based on continuum hypothesis. Taking these limitations in consideration, the present work is concerned with the modelling and the analysis of a slip flow through a rough curved microchannel. This is a first-time attempt to develop a perturbation solution, which predicts a slip flow behaviour in a rough curved microchannel, through the underlying physical and geometrical parameters. This study is relevant to the designing of curved microchannels and the optimisation of transport processes through rough microchannels characterised by curvature. In this paper, we assume that the flow is incompressible and isothermal. The roughness is considered to be sinusoidal with small amplitude. The rough walls are aligned with arbitrary phase difference between the outer and the inner rough walls. A continuum approach is adopted within the flow domain, such that the Navier–Stokes equations validly govern the incompressible flow. However, a non-continuum approach is proposed to describe the slip effects at the walls of the flow domain, for low Knudsen number.

The paper is partitioned as follows: In Sect. 2, the flow problem is modelled, and a domain perturbation technique is used to obtain the analytical expression for the volumetric flow rate of the problem. This procedure is under the assumption of small amplitude of the surface roughness relative to the distance between the curved walls. In Sect. 3, the analytical result is discussed as a functional dependence on the physical and geometrical parameters. The pertaining conclusion is given in Sect. 4.

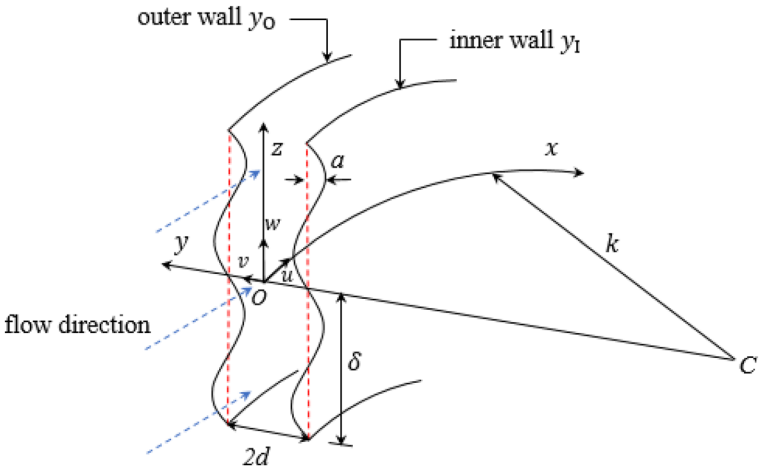

Fig. 1 Flow schematic

2 Theoretical and mathematical analysis

The flow schematic given in Fig. 1 describes a viscous flow within two rough curved walls with slip effects. The curved walls are separated by distance $2d$, and the surface roughness is taken to be sinusoidal in form. The channel radius of curvature is denoted by k, and (x, y, z) constitutes an orthogonal curvilinear coordinate system. The centre of the curved microchannel is at O. The width of the microchannel is constant along x, but varies periodically along z. The curved walls are positioned along the y-direction at

$$y = y_O = d + a\sin(2\pi z/\delta) \quad \text{and} \quad y = y_I = -d + a\sin(2\pi z/\delta + \varsigma), \tag{1}$$

where y_O and y_I describe the outer and the inner rough walls, respectively. The amplitude of the roughness is denoted by a, the roughness wavenumber by δ and ς is the phase difference between the rough curved walls, such that, $\varsigma = 0$, $0 < \varsigma < \pi$, and $\varsigma = \pi$ correspond to the in-phase, out-of-phase and the completely out-of-phase alignments of the outer and inner rough curved walls, respectively, see Fig. 2. The governing equations for the steady incompressible flow, taking the Stokes approximation [25–28], can be expressed as:

$$\nabla \cdot \hat{u} = 0, \tag{2}$$

$$\nabla \cdot \mathbb{T} - \nabla p = 0, \tag{3}$$

The mass and the momentum conservation equations are Eqs. (2) and (3), respectively, where $\hat{u} = u\hat{x} + v\hat{y} + w\hat{z}$ is the velocity vector, with $\hat{x}$, $\hat{y}$, and $\hat{z}$ as the unit vectors in the x-, y- and z-directions, respectively. p is the pressure, $\mathbb{T}$ is the stress tensor, and ∇ represents the gradient operator. In the slip regime, the velocity distribution satisfies Eqs. (2) and (3), but not the continuum wall conditions [25, 26], due to the slip effects at the walls. Thus, the Maxwellian equations specifying the slip effects at the rough walls of the curved microchannel can be expressed for the outer and inner walls, respectively, as

$$\hat{u} \cdot \hat{x} = -\frac{\lambda(2-\sigma)}{\mu\sigma}\left(\frac{\nabla(y - y_O)}{|\nabla(y - y_O)|} \cdot \mathbb{T}\right) \cdot \hat{x}, \tag{4}$$

$$\hat{u} \cdot \hat{x} = \frac{\lambda(2-\sigma)}{\mu\sigma}\left(\frac{\nabla(y - y_I)}{|\nabla(y - y_I)|} \cdot \mathbb{T}\right) \cdot \hat{x}, \tag{5}$$

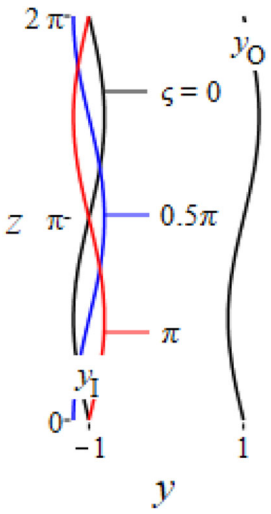

Fig. 2 Normalised representation of the phase difference ς between the outer y_O and the inner y_I rough walls

The constant μ is the dynamic viscosity. The mean free path is defined by λ, and σ is the tangential momentum accommodation coefficient, which can be assumed to be unity for many practical applications [17, 21].

Suppose the flow is generated by a pressure gradient $-\mathrm{d}p/\mathrm{d}x = G$ with velocity $\hat{u} = u(y, z)\hat{x}$; the lengths can be normalised by d, the pressure gradient by G, and the velocity by Gd^2/μ. Thus, the dimensionless wall slip conditions (Eqs. (4) and (5)) become

$$\begin{pmatrix} u|_{y=y_O} \\ u|_{y=y_I} \end{pmatrix} = \mathrm{Kn} \begin{pmatrix} -1 + \frac{1}{2}\varepsilon^2\alpha^2\cos^2(\alpha z) + \mathcal{O}(\varepsilon^3) & \varepsilon\alpha\cos(\alpha z) \\ 1 - \frac{1}{2}\varepsilon^2\alpha^2\cos^2(\alpha z + \varsigma) + \mathcal{O}(\varepsilon^3) & -\varepsilon\alpha\cos(\alpha z + \varsigma) \end{pmatrix} \begin{pmatrix} \mathbb{t}_{yx}|_{y=y_O} \\ \mathbb{t}_{zx}|_{y=y_I} \end{pmatrix}, \tag{6}$$

where $\mathbb{t}_{yx} = \partial_y u - (y + k)^{-1}u$, and $\mathbb{t}_{zx} = \partial_z u$ are the stresses, and $\partial_i \mathfrak{g}$ denotes the derivative of the function $\mathfrak{g}$ with respect to the variable i. The constant $\varepsilon = a/d$ is the dimensionless roughness amplitude, and Eq. (6) holds for small amplitude of the surface roughness relative to the channel width, i.e., $a \ll d$. For $\varepsilon = 0$, the complex wall conditions break down to the much simpler wall conditions of a smooth curved channel slip flow, without wall roughness. The dimensionless roughness wavenumber is denoted by $\alpha = 2\pi d/\delta$. Finally, $\mathrm{Kn} = \lambda/d$ is the Knudsen number, which gives the ratio of the mean free path to the characteristic width of the channel. The Knudsen number considered here is in the range $0.001 < \mathrm{Kn} \leq 0.1$. Therefore, we can now conveniently write the dimensionless governing equations for the flow as

$$\partial_x u = 0,$$

$$\big((y + k)\partial_y\big((y + k)\partial_y\big) + (y + k)^2\partial_{zz} - 1\big)u = -k(y + k), \tag{7}$$

with the wall slip conditions

$$u|_{y=y_O} = -\mathrm{Kn}\left(\left(1-\frac{1}{2}\varepsilon^2\alpha^2\cos^2(\alpha z)\right)\mathbb{t}_{yx} - \varepsilon\alpha\cos(\alpha z)\mathbb{t}_{zx}\right)\Big|_{y=y_O} + \mathcal{O}\left(\varepsilon^3\right),$$
$$u|_{y=y_I} = \mathrm{Kn}\left(\left(1-\frac{1}{2}\varepsilon^2\alpha^2\cos^2(\alpha z+\varsigma)\right)\mathbb{t}_{yx} - \varepsilon\alpha\cos(\alpha z+\varsigma)\mathbb{t}_{zx}\right)\Big|_{y=y_I} + \mathcal{O}\left(\varepsilon^3\right). \quad (8)$$

The streamwise velocity u depends on y and then z (due to the wall conditions, i.e., the periodic variation of the channel width along the z-direction, Fig. 2). For $\mathrm{Kn}\to 0$, the problem collapses into that of [25], where the velocity satisfies the no-slip conditions. For $k\to\infty$, the model of [20] for slip flow in a rough straight channel can be obtained. When $\varepsilon\to 0$ and $k\to\infty$, we get the model of slip flow in a smooth straight channel [30]. To obtain the analytical solution for small roughness amplitude, $\varepsilon \ll 1$, the regular perturbation expansion of the axial velocity is expressed as

$$u(y,z) = u^{(0)}(y) + \varepsilon u^{(1)}(y,z) + \varepsilon^2 u^{(2)}(y,z) + \mathcal{O}\left(\varepsilon^3\right). \quad (9)$$

Furthermore, any function $\mathfrak{g}$ can be Taylor expanded as:

$$\mathfrak{g}|_{y=y_O} = \mathfrak{g}|_{y=1} + \varepsilon\sin(\alpha z)\,\partial_y\mathfrak{g}\big|_{y=1} + \frac{1}{2}\varepsilon^2\sin^2(\alpha z)\,\partial_{yy}\mathfrak{g}\big|_{y=1} + \mathcal{O}\left(\varepsilon^3\right), \quad (10)$$
$$\mathfrak{g}|_{y=y_I} = \mathfrak{g}|_{y=-1} + \varepsilon\sin(\alpha z+\varsigma)\,\partial_y\mathfrak{g}\big|_{y=-1} + \frac{1}{2}\varepsilon^2\sin^2(\alpha z+\varsigma)\,\partial_{yy}\mathfrak{g}\big|_{y=-1} + \mathcal{O}\left(\varepsilon^3\right). \quad (11)$$

The procedure in Eqs. (10) and (11) can be used to expand the wall conditions in Eq. (8). Therefore, Taylor expanding Eq. (8) and using Eq. (9) in Eqs. (7) and (8), the terms of the same order in ε are grouped to obtain the following perturbation problems;

2.1 $\mathcal{O}$ (1) problem

The zeroth-order equation with the wall conditions is

$$(y+k)\partial_y\left((y+k)\partial_y u^{(0)}\right) - u^{(0)} = -k(y+k),$$
$$u^{(0)}\Big|_{y=1} = -\mathrm{Kn}\Big[(y+k)\partial_y((y+k)^{-1}u^{(0)})\Big]_{y=1},$$
$$u^{(0)}\Big|_{y=-1} = \mathrm{Kn}\Big[(y+k)\partial_y((y+k)^{-1}u^{(0)})\Big]_{y=-1}, \quad (12)$$

the exact solution of Eq. (12) is obtained as

$$u^{(0)}(y) = A_0(y+k) + A_1(y+k)^{-1} + \frac{1}{4}k(y+k)(1-2\ln(y+k)). \quad (13)$$

Equation (13) describes the velocity distribution for the slip flow in a smooth curved microchannel. The expressions of $A_{0,1}$ are given in Appendix B.

2.2 $\mathcal{O}$ (ε) problem

The first-order problem with the wall conditions can be written as

$$(y+k)\partial_y\left((y+k)\partial_y u^{(1)}\right) + (y+k)^2\partial_{zz}u^{(1)} - u^{(1)} = 0,$$
$$u^{(1)}\Big|_{y=1} + \sin(\alpha z)\,\partial_y u^{(0)}\Big|_{y=1} = -\mathrm{Kn}\Big[(y+k)\partial_y\left((y+k)^{-1}u^{(1)}\right) + \sin(\alpha z)\partial_y\left((y+k)\partial_y\left((y+k)^{-1}u^{(0)}\right)\right)\Big]_{y=1},$$

$$u^{(1)}\Big|_{y=-1} + \sin(\alpha z+\varsigma)\,\partial_y u^{(0)}\Big|_{y=-1} = \mathrm{Kn}\Big[(y+k)\partial_y\Big((y+k)^{-1}u^{(1)}\Big) + \sin(\alpha z+\varsigma)\partial_y\Big((y+k)\partial_y\Big((y+k)^{-1}u^{(0)}\Big)\Big)\Big]_{y=-1}, \tag{14}$$

the form of Eq. (14) suggests the solution

$$u^{(1)}(y,z) = g_1(y)\sin(\alpha z) + g_2(y)\cos(\alpha z). \tag{15}$$

Substituting Eq. (15) in Eq. (14) (see Appendix A) and solving the resulting equations give the following expressions for the functions $g_1(y)$ and $g_2(y)$;

$$g_1(y) = A_2 I_1(\alpha(y+k)) + A_3 K_1(\alpha(y+k)), \tag{16}$$

$$g_2(y) = A_4 I_1(\alpha(y+k)) + A_5 K_1(\alpha(y+k)), \tag{17}$$

where I_1 and K_1 are modified Bessel functions of order one and of the first and the second kind, respectively. Equation (15) with Eqs. (16) and (17) is the first-order correction to the velocity of the slip flow with roughness effect. The expressions of A_{2-5} are given in Appendix B.

2.3 $\mathcal{O}(\varepsilon^2)$ problem

The second-order problem reads

$$(y+k)\partial_y\Big((y+k)\partial_y u^{(2)}\Big) + (y+k)^2\partial_{zz}u^{(2)} - u^{(2)} = 0,$$

$$\begin{aligned}
&u^{(2)}\Big|_{y=1} + \sin(\alpha z)\,\partial_y u^{(1)}\Big|_{y=1} + \frac{1}{2}\sin^2(\alpha z)\,\partial_{yy}u^{(0)}\Big|_{y=1} \\
&= -\mathrm{Kn}\Bigg[(y+k)\partial_y\Big((y+k)^{-1}u^{(2)}\Big) \\
&\quad + \sin(\alpha z)\partial_y\Big((y+k)\partial_y\Big((y+k)^{-1}u^{(1)}\Big)\Big) \\
&\quad + \frac{1}{2}\sin^2(\alpha z)\partial_{yy}\Big((y+k)\partial_y\Big((y+k)^{-1}u^{(0)}\Big)\Big) \\
&\quad - \alpha\cos(\alpha z)\Big(\partial_z u^{(1)} + \frac{1}{2}\alpha\cos(\alpha z)(y+k)\partial_y\Big((y+k)^{-1}u^{(0)}\Big)\Big)\Bigg]_{y=1} \\
&u^{(2)}\Big|_{y=-1} + \sin(\alpha z+\varsigma)\,\partial_y u^{(1)}\Big|_{y=-1} + \frac{1}{2}\sin^2(\alpha z+\varsigma)\,\partial_{yy}u^{(0)}\Big|_{y=-1} \\
&= \mathrm{Kn}\Big[(y+k)\partial_y\Big((y+k)^{-1}u^{(2)}\Big) \\
&\quad + \sin(\alpha z+\varsigma)\partial_y\Big((y+k)\partial_y\Big((y+k)^{-1}u^{(1)}\Big)\Big) \\
&\quad + \frac{1}{2}\sin^2(\alpha z+\varsigma)\partial_{yy}\Big((y+k)\partial_y\Big((y+k)^{-1}u^{(0)}\Big)\Big) \\
&\quad - \alpha\cos(\alpha z+\varsigma)\Big(\partial_z u^{(1)} \\
&\quad + \frac{1}{2}\alpha\cos(\alpha z+\varsigma)(y+k)\partial_y\Big((y+k)^{-1}u^{(0)}\Big)\Big)\Big]_{y=-1},
\end{aligned} \tag{18}$$

at this order of approximation, we have a superposition of a periodic solution and non-periodic solution in z, namely:

$$u^{(2)}(y,z) = g_3(y) + g_4(y)\sin(2\alpha z) + g_5(y)\cos(2\alpha z). \tag{19}$$

Since we are interested in calculating a nonzero volumetric flow rate per unit cross-sectional area, $\{(y,z)|\ y_{\mathrm{I}} \le y \le y_{\mathrm{O}},\ 0 \le z \le 2\pi/\alpha\}$, the periodic parts of Eq. (19) can be ignored. Thus, substituting Eq. (19) in Eq. (18) (also see Appendix A) and solving gives the expression for the function $g_3(y)$ as

$$g_3(y) = A_6(y+k)^{-1} + A_7(y+k). \tag{20}$$

For the expressions of $A_{6,7}$, see Appendix B.

2.4 Volumetric flow rate

We define the dimensionless volumetric flow rate per unit cross-sectional area as

$$Q(\alpha,\varsigma,k,\mathrm{Kn}) = \frac{\alpha}{2\pi}\int_0^{2\pi/\alpha}\int_{y_{\mathrm{I}}}^{y_{\mathrm{O}}} u(y,z)\mathrm{d}y\mathrm{d}z. \tag{21}$$

The integral (Eq. (21)) using Taylor expansion about the unperturbed walls $y = -1$ and $y = 1$ can be analytically expressed up to second order in ε as

$$\begin{aligned}
Q(\alpha,\varsigma,k,\mathrm{Kn}) &= \int_0^{2\pi/\alpha}\int_{y_{\mathrm{I}}}^{y_{\mathrm{O}}} u(y,z)\mathrm{d}y\mathrm{d}z \\
&= \int_{-1}^{1} u^{(0)}(y)\mathrm{d}y + \varepsilon\frac{\alpha}{2\pi}\int_0^{2\pi/\alpha}\int_{-1}^{1} u^{(1)}(y,z)\mathrm{d}y\mathrm{d}z \\
&\quad + \varepsilon^2\frac{\alpha}{2\pi}\left[\int_0^{2\pi/\alpha}\int_{-1}^{1} u^{(2)}(y,z)\mathrm{d}y\mathrm{d}z\right. \\
&\quad + \int_0^{2\pi/\alpha}\left(\sin(\alpha z)\,u^{(1)}(y,z)\Big|_{y=1} - \sin(\alpha z+\varsigma)\,u^{(1)}(y,z)\Big|_{y=-1}\right)\mathrm{d}z \\
&\quad \left.+\frac{1}{2}\int_0^{2\pi/\alpha}\left(\sin^2(\alpha z)\,\partial_y u^{(0)}(y)\Big|_{y=1} - \sin^2(\alpha z+\varsigma)\,\partial_y u^{(0)}(y)\Big|_{y=-1}\right)\mathrm{d}z\right] \\
&\quad + \mathcal{O}\left(\varepsilon^4\right).
\end{aligned} \tag{22}$$

Evaluating Eq. (22), we obtain the analytical expression for the volumetric flow rate as

$$Q(\alpha,\varsigma,k,\mathrm{Kn}) = q(k,\mathrm{Kn})\left(1+\varepsilon^2\chi(\alpha,\varsigma,k,\mathrm{Kn}) + \mathcal{O}\left(\varepsilon^4\right)\right), \tag{23}$$

where

$$q(k,\mathrm{Kn}) = 2A_0k + A_1\ln\left(\frac{k+1}{k-1}\right) + \frac{1}{4}k\left[(k+1)^2(1-\ln(k+1)) - (k-1)^2(1-\ln(k-1))\right], \tag{24}$$

and

$$\begin{aligned}
&\chi(\alpha, \varsigma, k, \mathrm{Kn}) \\
&= \frac{1}{q}\left\{\frac{1}{4}\left[-A_1\frac{4k}{\left(k^2-1\right)^2} - \frac{1}{2}k\ln\left(\frac{k+1}{k-1}\right)\right] - \frac{1}{2}A_2\cos(\varsigma)I_1(\alpha(k-1))\right. \\
&\quad - \frac{1}{2}A_3\cos(\varsigma)K_1(\alpha(k-1)) + \frac{1}{2}A_2 I_1(\alpha(k+1)) + \frac{1}{2}A_3 K_1(\alpha(k+1)) \\
&\quad - \frac{1}{2}A_4\sin(\varsigma)I_1(\alpha(k-1)) - \frac{1}{2}A_5\sin(\varsigma)K_1(\alpha(k-1)) + A_6\ln\left(\frac{k+1}{k-1}\right) \\
&\quad \left.+2A_7 k\right\}
\end{aligned} \tag{25}$$

The expression in Eq. (23) gives the quantitative relation between the volumetric flow rate Q through the rough curved channel and volumetric flow rate q through a smooth curved channel without roughness. The function χ is the roughness function, which determines the effect of the roughness on the volumetric flow rate Q up to $\mathcal{O}\left(\varepsilon^2\right)$.

3 Results and discussion

The expression of the volumetric flow rate is obtained in the previous section as a function of α, ς, k and Kn. For small roughness amplitude, the effects of the channel geometry (i.e., α, ς, and k) and the wall slip (i.e., Kn) on the flow are discussed via graphical representations of the analytical solution. For a slip flow through a smooth curved channel without roughness ($\varepsilon = 0$), the volumetric flow rate q is illustrated in Fig. 3. The effect of the wall slip on the flow is evident when compared to the continuum flow: The volumetric flow increases with the Knudsen number Kn, for a given radius of curvature k. Furthermore, the volumetric flow rate increases with k.

For sufficiently large k, i.e., $k \to \infty$, the present analytical result is validated with the results (dash lines) in the literature. Firstly, when $\mathrm{Kn} = 0$, the result in Fig. 2 agrees with volumetric flow rate through a smooth straight channel, without wall slip (Poiseuille flow, [29]). Secondly, when $\mathrm{Kn} = 0.1$, the graphical result agrees with the result for the case of a slip flow in a smooth straight channel [20, 30].

For a slip flow through a rough curved microchannel ($0 < \varepsilon \ll 1$), the effects of the roughness can be discussed through the roughness function $\chi(\alpha, \varsigma, k, \mathrm{Kn})$, bearing in mind that the function $q(k, \mathrm{Kn})$ is always positive from Eq. (24) and Fig. 3. Therefore, by Eq. (23), the entire volumetric flow rate through the rough curved microchannel is augmented for $\chi > 0$, but not otherwise.

The effect of the roughness function χ on the slip flow as a function of the roughness wavenumber α is given in Fig. 4, taking a fixed Kn and different k and ς. The function χ is positive for small α (long wavelength of roughness), thus increasing the flow rate in the streamwise direction. On the other hand, for sufficiently large α (short wavelength of roughness), the function χ goes negative, thereby decreasing the flow rate consequently. This is because, the flow resistance imposed by the roughness increases with the increase in α. In addition, Fig. 4 reveals that the magnitude of the function χ increases with the radius

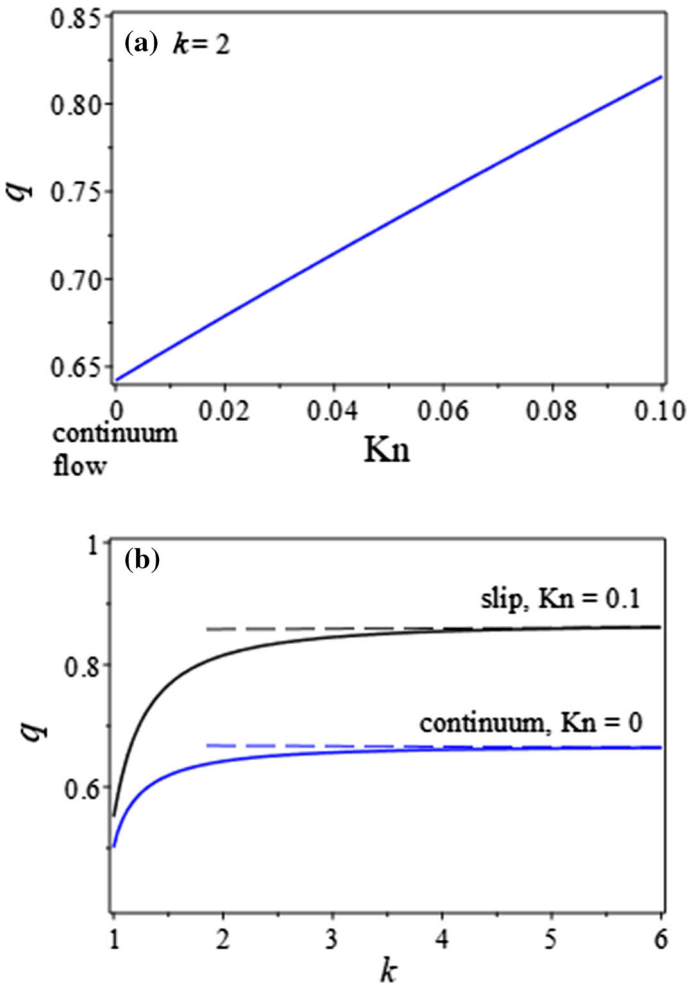

Fig. 3 Variation of the volumetric flow rate in a smooth channel, as function of the radius of curvature k, and the Knudsen number Kn. The dashed lines denote the results of a smooth straight channel ($k \to \infty$)

of curvature k in the presence of wall slip. This indicates that a slip flow in a rough straight channel may experience more roughness effect, compared to a rough curved channel. On comparing the profiles corresponding to the several alignments of the outer and inner rough curved walls (i.e., $\varsigma = 0$, $\varsigma = 0.5\pi$ and $\varsigma = \pi$), the flow resistance is relatively lesser when the outer and the inner rough curved walls are totally out-of-phase ($\varsigma = \pi$). This is clearly indicated in Fig. 4, which shows the function χ increasing with the phase difference ς between the rough curved walls. This implies that a maximum flow augmentation for the slip flow can be achieved by ensuring a phase difference of π between the two rough curved walls and small α. However, It would be impossible to augment the flow for large α, since the flow rate is always decreased in this case, because $\chi < 0$.

More information on the flow behaviour can be elucidated from Fig. 5. This shows that for all α, the of the magnitude of the function χ decreases when Kn is increased. This implies that the velocity slip at the walls decreases the roughness function, which specifies the effect of roughness on the volumetric flow rate. Physically, the increase in the Knudsen number

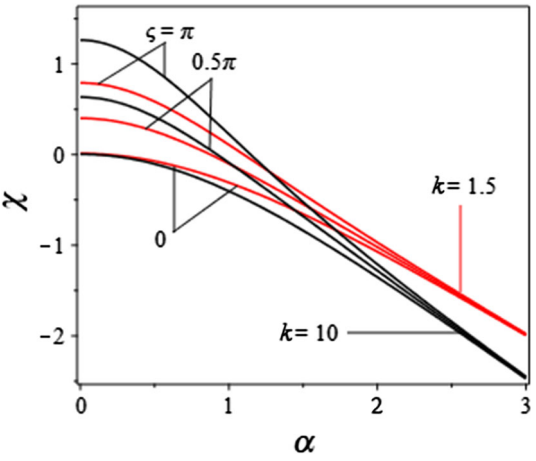

Fig. 4 Variation of the roughness function χ, as a function of the wavenumber α, for different phase difference ς and radius of curvature k, when Kn $= 0.1$

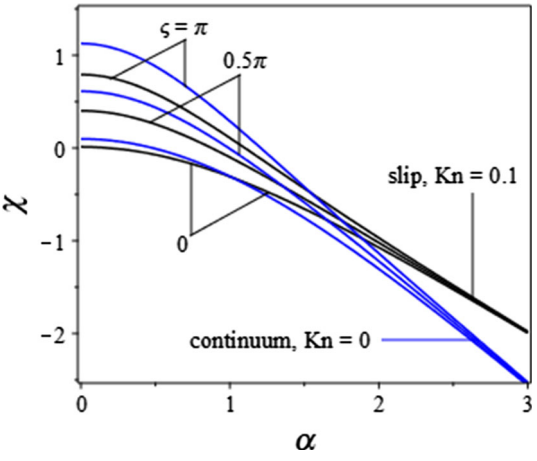

Fig. 5 Variation of the roughness function χ, as a function of the wavenumber α, for different phase difference ς, when $k = 1.5$

increases the effect of rarefaction on the flow; consequently, the fluid–wall interactions due to the rarefaction decreases the surface roughness effect. A common feature to Figs. 4 and 5 is the invariance of the roughness function χ for $\varsigma \geq 0$, when α is large. Therefore, the alignment of the rough curved walls does not matter, when the roughness wavenumber is large, for a slip flow as well as a continuum flow. The result for continuum flow, Kn $= 0$ result agrees with [25, 28].

Now, to show the effects of the slip and the roughness on the flow, from the perspective of χ as a function k, Figs. 6 and 7 are considered. In Fig. 6, when $\alpha = 0.4$, the function χ is only positive when the two rough curved walls are out-of-phase ($\varsigma > 0$) for all k, irrespective of Kn. The function χ increases with k for $\varsigma > 0$ and attains a constant behaviour ultimately for large k. On the contrary, when the walls are in-phase ($\varsigma = 0$), the function χ slightly increases with k initially, but decreases later to a constant, below zero. When $\alpha = 4$, as shown in Fig. 7, the function χ decreases below zero, for both Kn $= 0$ and Kn $= 0.1$. In general, for a given α, the magnitude of the roughness function χ is relatively greater for the continuum flow for, all ς and k. Figure 6 also reasserts that the alignment of the rough curved walls defined by ς has no effect on the flow when the roughness wavenumber is large enough, since the

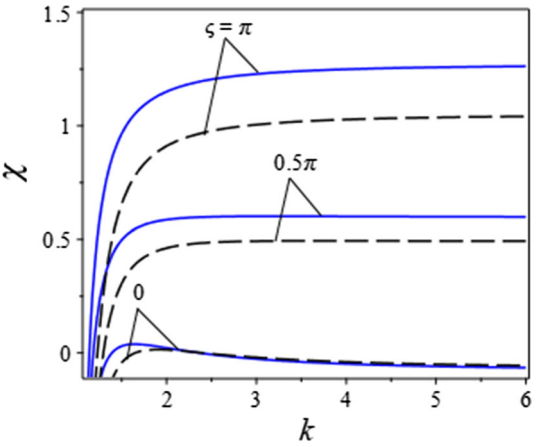

Fig. 6 Variation of the roughness function χ, as a function of the radius of curvature k, for continuum (Kn = 0, solid lines) and slip (Kn = 0.1, dashed lines) flows, and for different phase difference ς, when $\alpha = 0.4$

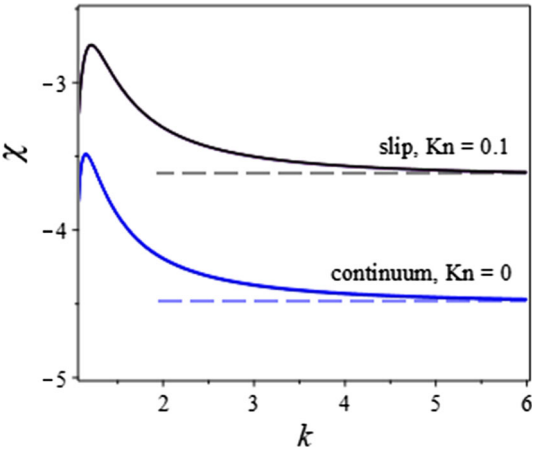

Fig. 7 Variation of the roughness function χ, as a function of the radius of curvature k, for different phase difference ς, when $\alpha = 4$

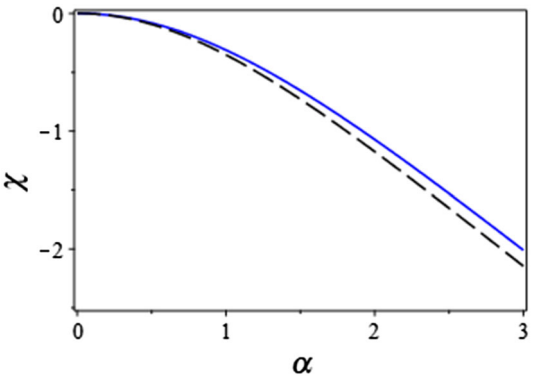

Fig. 8 Comparison with the result of [20], when $k = 15$ and $\varsigma = 0$, for continuum (Kn = 0, solid line) and slip (Kn = 0.1, dashed line) flows

curves show no variation with ς. We can also see that the curves reach the asymptotes, i.e., the dashed lines, which represent the roughness function for a rough straight microchannel ($k \to \infty$) for both the slip and the continuum flows.

In particular, we have also provided Fig. 8, to compare the present analytical result with the slip flow through a rough straight channel [20], which is a special case, for $k \to \infty$. The graph shows that the roughness function decreases when Kn is increased, for k sufficiently large, this agrees with [20].

4 Conclusions

A model is proposed for a slip flow through a curved microchannel with rough walls. The physical and geometrical effects neglected for microchannel flows, i.e., [20, 25] are considered in the present study. For small roughness amplitude, the domain perturbation method is systematically used to obtain the expression of the volumetric flow rate through the complex flow domain. The obtained results are validated with the limiting results in the literature

We have shown that the channel radius of curvature determines the volumetric flow rate, in addition to the roughness parameters. The roughness may augment the flow, for small roughness wavenumbers (long wavelength of roughness). For large wavenumbers (short wavelengths), the flow decreases eventually, due to the increase in the flow resistance. Another significant finding of the study is based on the comparison of the slip flow with the continuum flow: It is found that the roughness function which determines the roughness effect decreases with the increase in the Knudsen number of the slip flow. In the slip regime, the increase in the Knudsen number decreases the fluid–wall interactions. The model presented here can be used to understand and predict flows in rough curved microchannels, provided the wall roughness is small in amplitude and the Knudsen number is low. This study has practical applications in MEMS, where the design of microdomain for flows is utilised, and wall roughness is prevalent due to the limitations of the available fabrication techniques.

Appendix A

Differential equations

Substituting Eq. (15) in Eq. (14), we have the ordinary differential equations with the boundary conditions at $\mathcal{O}(\varepsilon)$;

$$
\begin{aligned}
&(y+k)^2\partial_{yy}g_1 + (y+k)\partial_y g_1 - \left(\alpha^2(y+k)^2+1\right)g_1 = 0,\\
&g_1|_{y=1} + \partial_y u^{(0)}\Big|_{y=1} = -\mathrm{Kn}\Big[(y+k)\partial_y\left((y+k)^{-1}g_1\right) + \partial_y\Big((y+k)\partial_y\Big((y+k)^{-1}u^{(0)}\Big)\Big)\Big]_{y=1},\\
&g_1|_{y=-1} + \cos(\varsigma)\,\partial_y u^{(0)}\Big|_{y=-1} = \mathrm{Kn}\Big[(y+k)\partial_y\left((y+k)^{-1}g_1\right)\\
&\quad + \cos(\varsigma)\partial_y\Big((y+k)\partial_y\Big((y+k)^{-1}u^{(0)}\Big)\Big)\Big]_{y=-1},
\end{aligned}
\tag{26}
$$

$$
\begin{aligned}
&(y+k)^2\partial_{yy}g_2 + (y+k)\partial_y g_2 - \left(\alpha^2(y+k)^2+1\right)g_2 = 0,\\
&g_2|_{y=1} = -\mathrm{Kn}\Big[(y+k)\partial_y\left((y+k)^{-1}g_1\right)\Big]_{y=1}.\\
&g_2|_{y=-1} + \sin(\varsigma)\,\partial_y u^{(0)}\Big|_{y=-1} = \mathrm{Kn}\Big[(y+k)\partial_y\left((y+k)^{-1}g_2\right)\\
&\quad + \sin(\varsigma)\partial_y\Big((y+k)\partial_y\Big((y+k)^{-1}u^{(0)}\Big)\Big)\Big]_{y=-1},
\end{aligned}
\tag{27}
$$

Substituting Eq. (19) in Eq. (18), we have the ordinary differential equation with the boundary conditions at $\mathcal{O}(\varepsilon^2)$;

$$
\begin{aligned}
&(y+k)^2\partial_{yy}g_3 + (y+k)\partial_y g_3 - g_3 = 0,\\
&g_3|_{y=1} + \frac{1}{2}\,\partial_y g_1\big|_{y=1} + \frac{1}{4}\,\partial_{yy}u^{(0)}\Big|_{y=1}\\
&= -\mathrm{Kn}\Bigg[(y+k)\partial_y\big((y+k)^{-1}g_3\big) + \frac{1}{2}\partial_y\big((y+k)\partial_y\big((y+k)^{-1}g_1\big)\big)\\
&\quad + \frac{1}{4}\partial_{yy}\Big((y+k)\partial_y\Big((y+k)^{-1}u^{(0)}\Big)\Big)\\
&\quad -\alpha^2\Big(\frac{1}{2}g_1 + \frac{1}{4}(y+k)\partial_y\Big((y+k)^{-1}u^{(0)}\Big)\Big)\Bigg]_{y=1},\\
&g_3|_{y=-1} + \frac{1}{2}\cos(\varsigma)\,\partial_y g_1\big|_{y=-1} + \frac{1}{2}\sin(\varsigma)\,\partial_y g_2\big|_{y=-1} + \frac{1}{4}\,\partial_{yy}u^{(0)}\Big|_{y=-1}\\
&= \mathrm{Kn}\Bigg[(y+k)\partial_y\big((y+k)^{-1}g_3\big) + \frac{1}{2}\cos(\varsigma)\partial_y\big((y+k)\partial_y\big((y+k)^{-1}g_1\big)\big)\\
&\quad + \frac{1}{2}\sin(\varsigma)\partial_y\big((y+k)\partial_y\big((y+k)^{-1}g_2\big)\big) + \frac{1}{4}\partial_{yy}\Big((y+k)\partial_y\Big((y+k)^{-1}u^{(0)}\Big)\Big)\\
&\quad -\alpha^2\Big(\frac{1}{2}\cos(\varsigma)g_1 + \frac{1}{2}\sin(\varsigma)g_2 + \frac{1}{4}(y+k)\partial_y\Big((y+k)^{-1}u^{(0)}\Big)\Big)\Bigg]_{y=-1}.
\end{aligned}
\tag{28}
$$

Appendix B

Coefficients

The coefficients for the perturbation solutions are expressed as follows

$$B_0 = 8k^2(\mathrm{Kn}+1) + 8(6\mathrm{Kn}-1), \tag{29}$$

$$
\begin{aligned}
B_1 = 4\big(k^2-1\big)^2(&-((k-2\mathrm{Kn}+1)K_1(\alpha(k+1)) - \alpha\mathrm{Kn}K_0(\alpha(k+1))(k+1))(k+2\mathrm{Kn}\\
&-1)I_1(\alpha(k-1))\\
&+(k-2\mathrm{Kn}+1)((k+2\mathrm{Kn}-1)K_1(\alpha(k-1))\\
&+\alpha\mathrm{Kn}K_0(\alpha(k-1))(k-1))I_1(\alpha(k+1))\\
&+\alpha\mathrm{Kn}(I_0(\alpha(k+1))(k+1)(k+2\mathrm{Kn}-1)K_1(\alpha(k-1))\\
&+(I_0(\alpha(k-1))(k-2\mathrm{Kn}+1)K_1(\alpha(k+1))\\
&-\alpha\mathrm{Kn}(I_0(\alpha(k-1))K_0(\alpha(k+1)) - I_0(\alpha(k+1))K_0(\alpha(k-1)))(k\\
&+1))(k-1))),
\end{aligned}
\tag{30}
$$

$$
\begin{aligned}
B_2 = 4(k-1)^2(&-((k-2\mathrm{Kn}+1)K_1(\alpha(k+1)) - \alpha\mathrm{Kn}K_0(\alpha(k+1))(k+1))(k+2\mathrm{Kn}\\
&-1)I_1(\alpha(k-1))\\
&+(k-2\mathrm{Kn}+1)((k+2\mathrm{Kn}-1)K_1(\alpha(k-1)) + \alpha\mathrm{Kn}K_0(\alpha(k-1))\,(k\\
&-1)I_1(\alpha(k+1))\\
&+\alpha\mathrm{Kn}(I_0(\alpha(k+1))(k+1)(k+2\mathrm{Kn}-1)K_1(\alpha(k-1)) + (k\\
&-1)(I_0(\alpha(k-1))(k-2\mathrm{Kn}+1)K_1(\alpha(k+1))
\end{aligned}
$$

$$
\begin{aligned}
&- \alpha \mathrm{Kn}((I_0(\alpha(k-1))K_0(\alpha(k+1)) - I_0(\alpha(k+1))K_0(\alpha(k-1)))(k \\
&+1))), \qquad (31)
\end{aligned}
$$

$$
B_3 = 16k\left(k^2-1\right)^2\left((\mathrm{Kn}+1)k^2 + 3\mathrm{Kn} - 1\right) \qquad (32)
$$

$$
\begin{aligned}
A_0B_0 = &-(k-1)^3(1+k-2\mathrm{Kn})\ln(k-1) \\
&+ (2\mathrm{Kn}+k-1)\left((k+1)^3\ln(k+1) - 2k(1+k-2\mathrm{Kn})\right), \qquad (33)
\end{aligned}
$$

$$
A_1B_0 = \left(\left(k^2-1\right)\ln(k-1) - k^2\ln(k+1) - 2k\mathrm{Kn} + \ln(k+1)\right)\left(k^2-1\right)^2, \qquad (34)
$$

$$
\begin{aligned}
A_2B_1 = &(k-1)^2(k+2\mathrm{Kn}-1)\left(2k(k+1)^3\ln(k+1) + k^4 + k^3(3-4A_0)\right. \\
&+3k^2(1-4A_0) + k(1-12A_0+4A_1) - 4A_0 \\
&-4(4\mathrm{Kn}-1)A_1)K_1(\alpha(k-1)) \\
&-\cos(\varsigma)\left(2k(k-1)^3\ln(k-1) + k^4 - k^3(3+4A_0) + 3k^2(1+4A_0)\right. \\
&-k(1+12A_0-4A_1) + 4A_0 + 4(4\mathrm{Kn}-1)A_1)(k-2\mathrm{Kn} \\
&+1)(k+1)^2K_1(\alpha(k+1)) \\
&+\left((k-1)^3\left(2k(k+1)^3\ln(k+1) + k^4 + k^3(3-4A_0) + 3k^2(1-4A_0)\right.\right. \\
&+k(1-12A_0+4A_1) - 4A_0 - 4(4\mathrm{Kn}-1)A_1)K_0(\alpha(k-1)) \\
&+\cos(\varsigma)\left(2k(k-1)^3\ln(k-1) + k^4 - k^3(3+4A_0) + 3k^2(1+4A_0)\right. \\
&\left.\left.\left.-k(1+12A_0-4A_1) + 4A_0 + 4(4\mathrm{Kn}-1)A_1)(k+1)^3K_0(\alpha(k+1))\right)\alpha\mathrm{Kn}, \right. \qquad (35)
\end{aligned}
$$

$$
\begin{aligned}
A_3B_1 = &-(k-1)^2(k+2\mathrm{Kn}-1)\left(2k(k+1)^3\ln(k+1) + k^4 + k^3(3-4A_0)\right. \\
&+3k^2(1-4A_0) + k(1-12A_0+4A_1) - 4A_0 \\
&-4(4\mathrm{Kn}-1)A_1)I_1(\alpha(k-1)) \\
&+\cos(\varsigma)\left(2k(k-1)^3\ln(k-1) + k^4 - k^3(3+4A_0) + 3k^2(1+4A_0)\right. \\
&-k(1+12A_0-4A_1) + 4A_0 + 4(4\mathrm{Kn}-1)A_1)(k-2\mathrm{Kn} \\
&+1)(k+1)^2I_1(\alpha(k+1)) \\
&+\alpha\mathrm{Kn}\left((k-1)^3\left(2k(k+1)^3\ln(k+1) + k^4 + k^3(3-4A_0)\right.\right. \\
&+3k^2(1-4A_0) + k(1-12A_0+4A_1) - 4A_0 \\
&-4(4\mathrm{Kn}-1)A_1)I_0(\alpha(k-1)) \\
&+\cos(\varsigma)\left(2k(k-1)^3\ln(k-1) + k^4 - k^3(3+4A_0) + 3k^2(1+4A_0)\right. \\
&\left.\left.\left.-k(1+12A_0-4A_1) + 4A_0 + 4(4\mathrm{Kn}-1)A_1)(k+1)^3I_0(\alpha(k+1))\right)\right), \qquad (36)
\end{aligned}
$$

$$
\begin{aligned}
A_4B_2 = &\left(2k(k-1)^3\ln(k-1) + k^4 - k^3(3+4A_0) + 3k^2(1+4A_0)\right. \\
&-k(1+12A_0-4A_1) + 16\mathrm{Kn}A_1 + 4(A_0-A_1)) \\
&(-(k-2\mathrm{Kn}+1)K_1(\alpha(k+1)) + \alpha\mathrm{Kn}(k+1)K_0(\alpha(k+1)))\sin(\varsigma), \qquad (37)
\end{aligned}
$$

$$
\begin{aligned}
A_5B_2 = &\left(2k(k-1)^3\ln(k-1) + k^4 - k^3(3+4A_0) + 3k^2(1+4A_0)\right. \\
&-k(1+12A_0-4A_1) + 16\mathrm{Kn}A_1 + 4(A_0-A_1)) \\
&((k-2\mathrm{Kn}+1)I_1(\alpha(k+1)) + \alpha\mathrm{Kn}(k+1)I_0(\alpha(k+1)))\sin(\varsigma), \qquad (38)
\end{aligned}
$$

$$
\begin{aligned}
A_6B_3 = &-2\alpha(k-1)^3(k+1)^5(k+2\mathrm{Kn}-1)(A_2\cos(\varsigma) + A_4\sin(\varsigma))I_0(\alpha(k-1)) \\
&+2\alpha(k-1)^3(k+1)^5(k+2\mathrm{Kn}-1)(A_3\cos(\varsigma) + A_5\sin(\varsigma))K_0(\alpha(k-1))
\end{aligned}
$$

$$
\begin{aligned}
&+2(k-1)^2(k+1)^5(k+4\mathrm{Kn}-1)(A_2\cos(\varsigma)+A_4\sin(\varsigma))I_1(\alpha(k-1))\\
&+2(k-1)^2(k+1)^5(k+4\mathrm{Kn}-1)(A_3\cos(\varsigma)+A_5\sin(\varsigma))K_1(\alpha(k-1))\\
&+2\alpha A_2(k+1)^3(k-1)^5(k-2\mathrm{Kn}+1)I_0(\alpha(k+1))\\
&-2\alpha A_3(k+1)^3(k-1)^5(k-2\mathrm{Kn}+1)K_0(\alpha(k+1))\\
&-2A_2(k+1)^2(k-1)^5(k-4\mathrm{Kn}+1)I_1(\alpha(k+1))\\
&-2A_3(k+1)^2(k-1)^5(k-4\mathrm{Kn}+1)K_1(\alpha(k+1))\\
&+k\Big(2\alpha^2k^9\mathrm{Kn}+2k^7\big(1-2\alpha^2\mathrm{Kn}\big)+4\alpha^2k^6\mathrm{Kn}A_1-6k^5\big(1-\alpha^2\mathrm{Kn}\big)\\
&+4k^4A_1\big(\big(\alpha^2-6\big)\mathrm{Kn}-4\big)+2k^3\big(3-2\alpha^2\mathrm{Kn}\big)-20k^2\mathrm{Kn}A_1\big(\alpha^2+12\big)\\
&-k\big(2-\alpha^2\mathrm{Kn}\big)+\big(16+12\big(\alpha^2-10\big)\mathrm{Kn}\big)A_1\Big),
\end{aligned}
\tag{39}
$$

$$
\begin{aligned}
A_7B_3 = {}&2\alpha(k+1)^2(k-1)^3(k+2\mathrm{Kn}-1)(k-2\mathrm{Kn}+1)(A_2\cos(\varsigma)+A_4\sin(\varsigma))I_0(\alpha(k-1))\\
&-2\alpha(k+1)^2(k-1)^3(k+2\mathrm{Kn}-1)(k-2\mathrm{Kn}+1)(A_3\cos(\varsigma)+A_5\sin(\varsigma))K_0(\alpha(k-1))\\
&-2(k+1)^2(k-1)^2(k+4\mathrm{Kn}-1)(k-2\mathrm{Kn}+1)(A_2\cos(\varsigma)+A_4\sin(\varsigma))I_1(\alpha(k-1))\\
&-2(k+1)^2(k-1)^2(k+4\mathrm{Kn}-1)(k-2\mathrm{Kn}+1)(A_3\cos(\varsigma)+A_5\sin(\varsigma))K_1(\alpha(k-1))\\
&-2\alpha A_2(k-1)^2(k+1)^3(k+2\mathrm{Kn}-1)(k-2\mathrm{Kn}+1)I_0(\alpha(k+1))\\
&+2\alpha A_3(k-1)^2(k+1)^3(k+2\mathrm{Kn}-1)(k-2\mathrm{Kn}+1)K_0(\alpha(k+1))\\
&+2A_2(k-1)^2(k+1)^2(k+2\mathrm{Kn}-1)(k-4\mathrm{Kn}+1)I_1(\alpha(k+1))\\
&+2A_3(k-1)^2(k+1)^2(k+2\mathrm{Kn}-1)(k-4\mathrm{Kn}+1)K_1(\alpha(k+1))\\
&-k\Big(\alpha^2k^7\mathrm{Kn}+k^5\mathrm{Kn}\Big(\alpha^2(4\mathrm{Kn}-3)-2\Big)+4\alpha^2k^4\mathrm{Kn}A_1\\
&+k^3\mathrm{Kn}\Big(4+\alpha^2(3-8\mathrm{Kn})\Big)-8k^2A_1\Big(1+\Big(\alpha^2+2\Big)\mathrm{Kn}\Big)\\
&+k\mathrm{Kn}\Big(\alpha^2(4\mathrm{Kn}-1)-2\Big)+96\mathrm{Kn}^2A_1+4\mathrm{Kn}\Big(\alpha^2-20\Big)A_1+8A_1\Big).
\end{aligned}
\tag{40}
$$

References

1. P. Debye, R.L. Cleland, J. Appl. Phys. **30**, 843 (1959)
2. S.T. Cho, K.T. Wise, Sens. Actuat. A-Phys. **36**, 47 (1993)
3. M. Gadel Hak, J. Fluids Eng. **121**, 5 (1999)
4. Y. Huang, A. Sanli Ergun, E. Hæggström, M.H. Badi, B. Khuri-Yakub, J. Microelectromech. Syst. **12**, 128 (2003)
5. H.A. Stone, A.D. Stroock, A. Ajdari, Annu. Rev. Fluid Mech. **36**, 381 (2004)
6. D.J. Beebe, G.A. Mensing, G.M. Walker, Annu. Rev. Biomed. Eng. **4**, 261 (2002)
7. Y.L. Zhang, R.V. Craster, O.K. Matar, J. Colloid Interface Sci. **264**, 160 (2003)
8. S. Tison, Vacuum **44**, 1171 (1993)
9. P. Wu, W.A. Little, Cryogenics **23**, 273 (1983)
10. P. Wu, W.A. Little, Cryogenics **24**, 415 (1984)
11. J.C. Harley, Y. Huang, H.H. Bau, J.N. Zemel, J. Fluid Mech. **284**, 257 (1995)
12. X.F. Peng, G.P. Peterson, Int. J. Heat Mass Transf. **39**, 2599 (1996)
13. Z.X. Li, D.X. Du, Z.Y. Guo, Microscale Therm. Eng. **7**, 253 (2003)
14. W.A. Ebert, E.M. Sparrow, J. Basic Eng. **87**, 1018 (1965)
15. E.B. Arkilic, M.A. Schmidt, K.S. Breuer, J. Microelectromech. Syst. **6**, 167 (1997)
16. F.E. Larrade, C. Housiadas, Y. Drossino, Int. J. Heat Mass Transf. **40**, 2669 (2000)
17. S.A. Scha, P.L. Chambre, Flow of Rarefied Gases, *Fundamentals of Gas Dynamics* (Princeton University Press, New Jersey, 1958)

18. K.-H.W. Chu, Z. Angew. Math. Phys. **47**, 591 (1996)
19. W.L. Li, J.W. Lin, S.C. Lee, M.D. Chen, J. Micromech. Microeng. **12**, 149 (2002)
20. H. Sun, M. Faghri, Numer. Heat Transfer, Part A **43**, 1 (2003)
21. Z. Duan, Y.S. Muzychka, J. Fluid Eng. **130**, 031102 (2008)
22. R. Garg, A. Agrawal, SN Appl. Sci. **1**, 1035 (2019)
23. R. Garg, A. Agrawal, AIP Adv. **9**, 125114 (2019)
24. R. Garg, A. Agrawal, Phys. Fluids **32**, 052002 (2020)
25. N.F. Okechi, S. Asghar, Eur. Phys. J. Plus **134**, 165 (2019)
26. N.F. Okechi, S. Asghar, Eur. J. Mech. B. Fluids **84**, 81 (2020)
27. N.F. Okechi, S. Asghar, Eur. J. Mech. B. Fluids **84**, 15 (2020)
28. N.F. Okechi, S. Asghar, D. Charreh, AIP Adv. **10**, 035114 (2020)
29. F.M. White, *Viscous fluid flow* (McGraw-Hill, New York, 2006)
30. C. Shen, *Rarefied gas dynamics: fundamentals, simulation and micro flow* (Springer, Berlin, 2005)